SSRG International Journal of Electrical and Electronics Engineering
ISSN: 2348-8379/ https://doi.org/10.14445/23488379/IJEEE-V13I4P109

Volume 13 Issue 4, 119-132, April 2026

Original Article

An Efficient DL Based Segmentation Technique for Breast Ultrasound Images

Priyanshu Tripathi[1], Rajeshwar Dass[2], Jyotsna Sen[3]

[1,2]*ECED, D.C.R. Univ. of Sci. and Tech., Murthal, Haryana.*
[3]*Department of Radio-diagnosis, Pt. B. D. Sharma PGIMS, Rohtak, Haryana.*

[2]*Corresponding Author : rajeshwardass.ece@dcrustm.org*

Received: 18 January 2026 Revised: 27 February 2026 Accepted: 26 March 2026 Published: 30 April 2026

Abstract *- This paper presents an efficient and novel DL-based segmentation technique for Breast Ultrasonographic (BUS) Images. In the first step, BUS images are despeckled to get enhanced lesion texture and visibility. Further, an encoder-decoder-based segmentation algorithm is employed for the accurate detection of the boundary and textual information of the breast tissue. Various pre-existing despeckling filters are categorized into basic, smoothing, and edge-preserving filters, and their performance is evaluated using SEPI metrics. Finally, the efficient despeckling filters are fused to enhance performance. The fusion of the Bilateral Filter and Anisotropic Diffusion Filter (BiF-ADF) yields optimal performance according to the SEPI metrics. After despeckling, the filtered images are fed into a semantic segmentation module to segment lesions in the BUS images. In the segmentation module, various state-of-the-art DL-based algorithms are implemented using transfer learning, and their performance is evaluated based on the mean IOU. It is observed that the ResNet-50 model yielded a higher value. To further enhance the segmentation performance, an efficient technique, Clipped-ResNet50, is proposed, yielding the highest mean IOU values of 0.9089 and 0.9060, and accuracy of 0.9379 and 0.9387 for the BUSI and PGI Rohtak datasets, respectively. Further, Clipped-ResNet50 is also trained on despeckled, i.e., enhanced images, showing a notable improvement in segmentation outcomes. When applying the model to despeckled images, the mean IOU and accuracy increased from 90.89% to 93.05% and 90.60% to 92.89% for the BUSI and PGI Rohtak datasets, respectively, highlighting the significant advantage of using despeckled breast ultrasound images for segmentation tasks.*

Keywords *- Breast Ultrasonographic (BUS) Images, Speckle Noise, Despeckling Filters, SEPI metrics, Image Fusion, Semantic Segmentation, Mean IOU.*

1. Introduction

Breast cancer is the most commonly diagnosed cancer among women worldwide [1]. Breast cancer alone constitutes 25% of the malignant cases diagnosed in women globally [2]. Various imaging modalities, such as ultrasound, X-rays, CT, and MRI, can be employed for the diagnosis of breast lesions [3]. Ultrasonographic imaging modalities are extensively utilized in breast lesion diagnosis owing to their non-intrusive attributes, low cost, and harmless screening.

To diagnose any abnormalities in the internal part of the breast, the visual quality of the BUS images should be good. Speckle noise degrades the visual quality of BUS images, leading to inaccurate diagnosis. Therefore, different despeckling filters are used to reduce the impact of speckle noise [4]. Despeckling filters reduce noise in ultrasonographic images without causing edge blur. It attempts to identify complex edges and preserve them. An intrinsic characteristic of breast ultrasonography is speckle noise, which often tends to diminish image quality and contrast, which in turn lowers diagnostic information. Therefore, it is essential to reduce speckle noise from BUS images to improve the image quality and segmentation accuracy. Recent advances in deep learning, especially U-Net and ResNet-based models, have achieved promising results in medical image segmentation. However, there is a crucial research gap since most existing DL based BUS segmentation methods are employed on minimally processed images without integrating despeckling techniques to improve segmentation performance. Moreover, limited research has explored the fusion of multiple despeckling techniques and a unified framework of despeckling and segmentation. To address these challenges, this work proposed a novel and efficient DL based segmentation framework for BUS images. The key contributions are as follows:

Two datasets, BUSI and PGI Rohtak, are preprocessed for despeckling and segmentation of BUS images. An optimized despeckling algorithm (AD-BiF) is proposed by fusing information from two different filters, and its performance is

computed using the SEPI metric.Optimized segmentation algorithm (Clipped-ResNet50) by clipping the activation function (ReLu) and inserting a dropout layer in the ResNet50 model to avoid overfitting.

2. Literature Review

Various despeckling techniques have been employed in the analysis, segmentation, and classification of different medical imaging techniques. An overview of studies conducted by multiple scholars is listed in Table 1.

Table 1. Distinct studies of despeckling algorithms for ultrasonographic images

Author(s)	Year	Datasets	No. of images	Despeckling algorithms	Performance evolution metrics
Flore et al. [5]	2014	BUSI	900 & 50	5	FOM
Elyasi et al. [6]	2016	BUSI	3	11	PSNR, SNR, SSIM
Kriti et al. [7]	2019	BUSI	100	42	IQI, Beta, and Image Quality Metric
Choi et al. [8]	2020	BUSI	5	11	PSNR, SSIM, MSE
Ayana et al. [9]	2022	BUSI	250 & 6	4	PSNR, SSIM, MSE
Yadav et, al. [10]	2023	TUSI	820	64	IQI, Beta, and SEPI
Tong Ying et al. [11]	2024	BUSI	192	2	-
D. Jung et al. [12]	2024	Medical US	7776	3	PSNR, SSIM
X. Li et al. [13]	2025	US	-	9	PSNR, SSIM, CNR
M. Khalifa et al. [14]	2025	BUSI	780	7	PSNR, SSIM, FOM
M. S. Gokmen et al. [15]	2025	US	4226 & 4744	6	PSNR
N. Patil et al. [16]	2025	BUSI	780	4	PSNR, SSIM
V. S. Patil et al. [17]	2026	TUSI	134	6	CQE, PSNR, SSIM

Note- BUSI- Breast Ultrasound Images, TUSI- Thyroid Ultrasound Image, IQI- Image Quality Index, CQE- Color Quality Enhancement

3. Methodology

Figure 1 illustrates the methodology utilized for segmenting BUS images. The proposed methodology is elaborated step-by-step as follows:

3.1. Breast Ultrasonographic Images Dataset

In this research, the following two BUS datasets are used:

3.1.1. Dataset A (BUSI)

This dataset was introduced in 2018 and has 780 Breast Ultrasonographic Images (133 non-cancerous, 437 benign, and 210 malignant). A total of 647 of 780 images are used from this benchmark dataset. The ground truth images are also presented with the original images. For preprocessing purposes, all images are resized to 256×256 and 299×299 [18].

3.1.2. Dataset B (PGI Rohtak)

A Total of 105 (65 benign and 40 malignant) images were collected from the government hospital PGI Rohtak. These images were collected between 2021 and 2023, encompassing an age group of 25-70 years. These breast ultrasonographic images are also resized to 256×256 and 299×299 for preprocessing. Benign cases include masses with fibroadenomas, hypoechoic, simple anechoic, and complex anechoic, whereas malignant masses include hypoechoic and hyperechoic, ductal carcinoma, and dense masses with micro and macro calcifications.

3.2. Despeckling Filters

Despeckling filters remove speckle noise from ultrasonographic images. This noise is multiplicative and has a seed-like structure that complicates the analysis of breast images by radiologists.

Hence, an appropriate despeckling technique is required to minimize this noise while preserving the edges and overall structure of the Breast Ultrasonographic Images. Many researchers have proposed various techniques for reducing speckle noise [7, 10, 19, 20]. All the filters, that is, linear and non-linear, which are implemented in this work, are categorized into three categories: basic filters, smoothing filters, and edge-preserving filters.

3.2.1. Basic Filters

Lee, Frost, Kaun, Weiner, and wavelet filters are linear filters, and their operations are based on the mean and variance, except for the wavelet filter, which uses the wavelet transform. The median and bilateral filters are non-linear.

The bilateral filter replaces each pixel value with a weighted average of its neighboring pixels, where the weights are computed based on either spatial proximity or intensity similarity**.** Lee, Frost, Kaun, Median, Weiner, Bilateral, and Wavelet filters are categorized as basic filters [7, 19, 21, 22, 23].

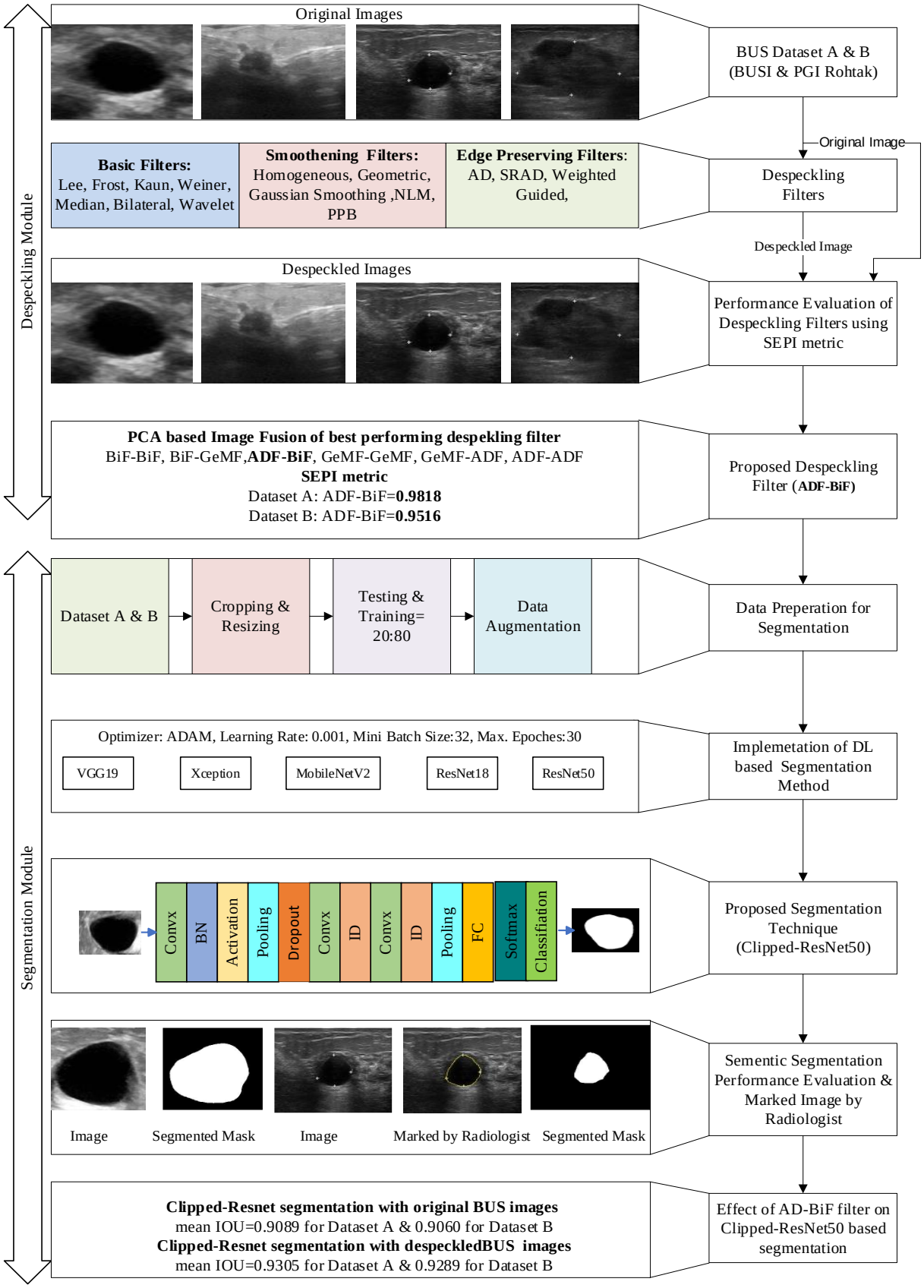

Fig. 1 Proposed methodology for segmentation of BUS images

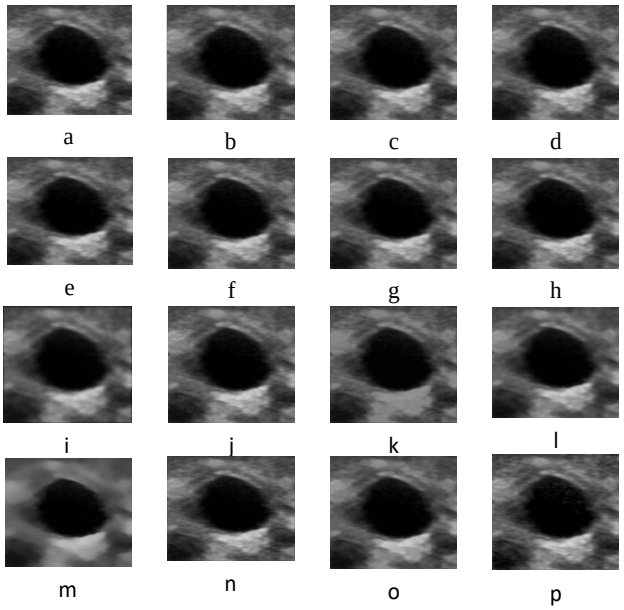

Fig. 2(a) Original BUS image of dataset-A, corresponding despeckled image by (b) Lee filter, (c) Kaun filter, (d) Frost filter, (e) Weiner filter, (f) Median filter, (g) Bilateral (BiF) filter, (h) Wavelet filter, (i) Homogeneous (Homog) filter (j) Geometric (GeM) filter (k) Gaussian smoothing (GS) filter, (l) Non Local Mean (NLM) filter, (m) Probability Patch Based (PPB) filter, (n) Anisotropic Diffusion (AD) filter, (o) Speckle Reduction Anisotropic Diffusion (SRAD) filter, (p) Weighted Guided (WG) filter.

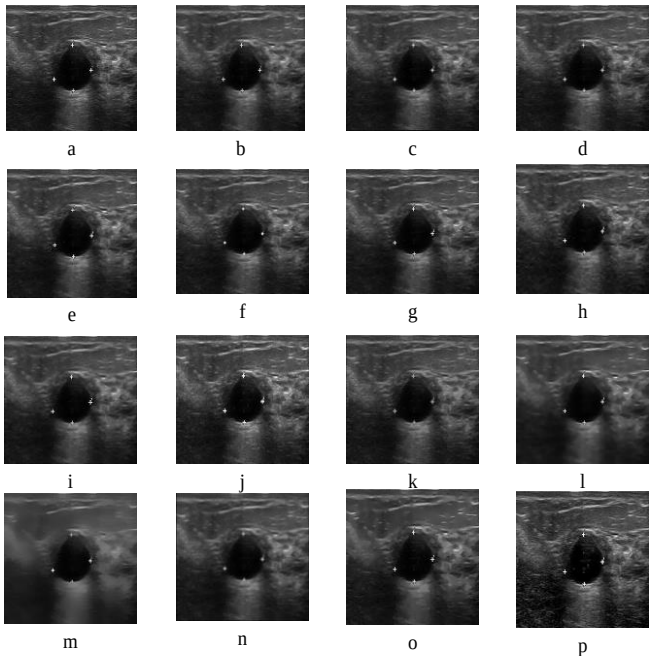

Fig. 3(a) Original BUS image of dataset-B, corresponding despeckled image by (b) Lee filter, (c) Kaun filter, (d) Frost filter, (e) Weiner filter, (f) Median filter, (g) Bilateral (BiF) filter, (h) Wavelet filter, (i) Homogeneous (Homog) filter (j) Geometric (GeM) filter (k) Gaussian smoothing (GS) filter, (l) Non Local Mean (NLM) filter, (m) Probability Patch Based (PPB) filter, (n) Anisotropic Diffusion (AD) filter, (o) Speckle Reduction Anisotropic Diffusion (SRAD) filter, and (p) Weighted Guided (WG) filter.

3.2.2. Smoothening Filters

Smoothening filters are based on their noise removal properties. These filters focus more on the smoothing operation. Homogeneous, Geometric, Gaussian smoothening, Non-Local Mean Filter (NLM), and Probability Patch-Based (PPB) filters are categorized as smoothening filters. Homogeneous, geometric, and Gaussian smoothing filters are linear filters that work on local statistics, whereas NLM and PPB filters are non-linear filters. The NLM filter works on a similarity window, and the PPB filter works on a probabilistic patch [7, 10, 19, 20].

3.2.3. Edge Preserving Filters

These filters are focused on their edge-preserving properties. The AD, SRAD, and Weighted Guided filters are categorized as edge-preserving filters. An Anisotropic Diffusion (AD) filter preserves edges by adapting local image content. In this study, the Perona-Malik diffusion filter is used in the AD filter [24-27]. The BUS images in their original and despeckled forms for Datasets A and B are presented in Figures 2 and 3, respectively.

3.3. Performance Analysis of Despeckling Filters

The performance evaluation of the despeckling filters is evaluated according to the image quality metrics. The various objective evaluation parameters used for the performance evaluation of the despeckling techniques are as follows:

The IQI is given by [7]

$$IQI = \frac{\sigma_{pq}}{\rho_p \rho_q} \cdot \frac{2\bar{p}\bar{q}}{\bar{p}^2+\bar{q}^2} \cdot \frac{2\sigma_p \rho_q}{\overline{\sigma_p}^2+\overline{\rho_q}^2} \quad (1)$$

where σ_{pq} denotes the covariance of the original and despeckled images, and ρ_p and ρ_q denote their respective standard deviations. $\bar{p}$ and $\bar{q}$ denote their respective mean values.

The β metric is given by [28]

$$\beta = \frac{\sum(\Delta h_p - \Delta\overline{h_q})(\Delta h_p - \Delta\overline{h_q})}{\sqrt{\sum(\Delta h_p - \Delta\overline{h_q})^2 . \sum(\Delta h_p - \Delta\overline{h_q})^2 .}} \quad (2)$$

where Δh_p and Δh_q are the high-pass-filtered values of the original and despeckled images, respectively the Structure & Edge Preserving Index (SEPI) is the average of IQI & β, and it is given as [10]:

$$SEPI = \frac{IQI+\beta}{2} \quad (3)$$

The BUS images are preprocessed using various basic despeckling filters, and it is noticed that the bilateral filter, geometric filter, and anisotropic diffusion filter yielded the highest value of SEPI metrics in their respective categories, as shown in Table 2.

4. BUS Image Fusion by Principal Component Analysis (PCA)

Image fusion is a method of integrating information from two different images. In this work, two breast ultrasonographic images despeckled by different filters are combined to fuse information. The fusion process is achieved by using principal component analysis. The algorithm for the PCA-based image fusion is derived from the principal component analysis method applied to the pixel values of the filtered input images. This process involves the following key steps:

Table 2. SEPI Metrics of distinct despeckling filters

Filter	Filter Name	Assessment Metrics (SEPI in μ±sd)	
		Dataset A	Dataset B
Basic Filters	Lee	0.9440±0.0622	0.8159 ±0.2014
	Frost	0.9603 ±0.0462	0.7958 ±0.2159
	Kaun	0.9234±0.0905	0.6488 ±0.3474
	Weiner	0.9604 ±0.0462	0.6879 ±0.3050
	Median	0.9603±0.0593	0.7646 ±0.2389
	Bilateral	0.9631 ± 0.0446	0.8669±0.1973
	Wavelet	0.9201±0.0857	0.7838 ±0.2207
Smoothening Filters	Homogeneous	0.8205±0.1841	0.7775 ±0.2105
	Geometric	0.9302 ± 0.093	0.8007±0.2377
	Gaussian Smoothing	0.9030±0.0896	0.7478 ±0.2521
	Non-Local Mean	0.9260±0.0878	0.7618 ±0.2381
	Probability Patch-Based	0.9105±0.0954	0.7209 ±0.2662
Edge Preserving Filters	Anisotropic Diffusion	0.9513 ± 0.0617	0.8542±0.1453
	SRAD	0.9206±0.1084	0.7879 ±0.2030
	Weighted Guided	0.8205±0.1841	0.7949 ±0.2159

Step 1: Arrange the given images m (j, k) and n (j, k) into a vector.

Step 2: Compute covariance matrices for each image vector.

Step 3: Compute the eigen vector for each image vector.

Step 4: The weights are calculated by normalizing the selected image eigenvector for the given input images.

Step 5: Compute the weighted sum by multiplying each pixel of the input image by its weight and adding them [29].

$$X(j,k) = w_g * m(j,k) + w_h * n(j,k) \quad (4)$$

Six hybrid despeckled filters, i.e., Bilateral-Bilateral (BiF-BiF), Bilateral-Geometric (BiF-SRADF), Bilateral-Anisotropic Diffusion (BiF-ADF), SRADF-SRADF, SRAD-AD, and AD-AD, are formulated by combining three filters: bilateral, AD, and geometric, due to their best performance in the categories as shown in Table 3.

The performance evaluation of all these filters is shown in Table 4, and the results indicate that the fusion of the AD filter and the Bilateral Filter (ADF-BiF) achieved the highest SEPI values for both datasets. The SEPI metrics evaluation is given in Table 3 for dataset A and dataset B, and the filtered BUS images with the original image of both datasets are depicted in Figure 4.

Table 3. SEPI metrics of different hybrid despeckling filters

Filter Name	Assessment Metrics (SEPI in μ±sd)	
	Dataset A	Dataset B
BiF-BiF Filter	0.9631 ±0.0446	0.8670 ±0.1972
BiF-GeMF Filter	0.9602 ±0.0486	0.8463 ±0.1532
ADF-BiF Filter	**0.9818 ± 0.0241**	**0.9516 ± 0.1859**
GeMF -GeMF Filter	0.9513 ±0.0617	0.8762 ±0.0217
GeMF-ADF Filter	0.9779 ±0.0265	0.8853 ±0.0047
ADF-ADF Filter	0.9806 ± 0.0259	0.9325 ± 0.0563

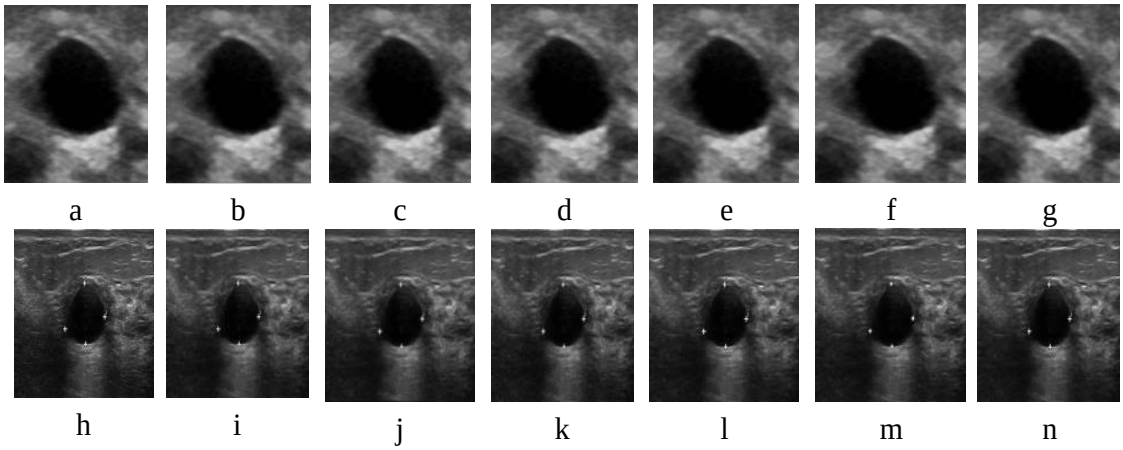

Fig.4 (a) Original image of dataset A, image despecked by (b) BiF-BiF filter, (c) BiF-GeMF filter, (d) AD-BiF filter, (e) GeMF-GeMF filter, (f) GeMF-ADF filter, (g) ADF-ADF filter, (h) Original Image of Dataset B, Image despecked by (i) BiF-BiF filter, (j) BiF-GeMF filter, (k) AD-BiF filter, (l) GeMF-GeMF filter, (m) GeMF-ADF filter, (n) ADF-ADF filter

5. Segmentation Module

After despeckling, the preprocessed BUS images are applied to semantic segmentation. Segmentation is a crucial step because it provides a precise lesion area that ensures proper classification. In this study, deep learning-based segmentation is performed.

Many DL-based techniques have been proposed by researchers in the literature for segmentation of BUS images, as shown in Table 4 [30-45]: Data Preparation for Segmentation. In this study, two datasets are utilized, as discussed in Section 2.1. Six hundred forty-seven images from dataset-A are cropped and resized to 256 × 256 for VGG19, ResNet18, ResNet50, and MobileNetV2, resized to 299 × 299 for Xception, and then divided into test and training datasets at a ratio of (20:80). A total of 130 images (65 benign and 65 malignant) are used for testing. The remaining 517 images (372 benign and 145 malignant) are augmented by rotation (90, 180, and 270 degrees) and translation.

This process results in a total of 13,366 images prepared for training and validation. A total of 12000 images (6000 benign and 6000 malignant) is used for training, and 1366 images (683 benign and 683 malignant) are utilized for validation.

Table 4. Existing research findings of segmentation methods for ultrasonographic images

S. No.	Author(s)	Year	No. of Images	Method(s)	Performance Parameter(s)
1	Samuel E. Johnny et al. [30]	2026	2500	SAM-based multi-task framework	Acc=92.3%, Dice=0.887
2	Yajuan Li et al. [31]	2025	526	ResNet34, MobileNetV3Small InceptionV3	Acc=82.4%, 87.0%, and 77.8%
3	Bruno et al. [32]	2025	780+266	Dual-stage DL Model	Dice: 0.92, Accuracy: 91.5%
4	Md Amanour Rahman [33]	2025	780	HyFormer-Net: synergistic CNN-Transformer	Dice: 0.761, Accuracy: 93.2%, IOU= 0.623
5	L. Boro et al. [34]	2024	-	CBAM-RIUnet	DSC=89.38% and IoU= 88.71%
6	G. Madhu et al. [35]	2024	100+780	Two-stage U-Net	DSC=80.71% and IoU= 68.53%
7	P. Pramanik et al. [36]	2024	163+780	PCBAM+SWA	DSC=73.97% and IoU= 65.23%
8	Hesaraki et al. [37]	2024	780	UNet++ + LSTM hybrid	Dice: 0.90, IoU: 0.84
9	Y. Lyu et al. [38]	2023	100+780	*AMS-PAN: Attention + Multi-Scale Pyramid Attention Network*.	Dice: 79.62%, IOU= 67.52%
10	H. Yang et al. [39]	2023	163+780	U-Net	IoU: 78.61, DSC: 87.25

11	Zhao et al. [40]	2022	-	U-Net	IoU:0.851, DSC: 0.921
12	Kim et al. [41]	2021`	1400	VGG16, ResNet34, and GoogLeNet	AUC:0.89, 0.86,0.90
13	Huang et al. [42]	2021	325+163+780	VGG16, ResNet101, PSPNet and Deeplab	IOU: 68.76, 75.35, 76.61, 71.58
14	Ilesanmi et al. [43]	2021	264+830	U-Net, Segnet	DSC=91.88
15	Flores et al. [44]	2020	3061	Alexnet U-Net, VGG16, VGG19, Resnet-18, Resnet-50, Mobilenet, Xception	IOU: 0.73, 0.804, 0.819, 0.826, 0.827, 0.832, 0.823, 0.821

5.1. DL based Segmentation Method(s)

Here, different DL-based segmentation models are implemented, viz, VGG19, ResNet18, ResNet50, MobileNetV2, Xception, for segmentation of BUS images. Further, a Clipped ResNet50, DL-based segmentation model is proposed for segmentation of BUS images, and its performance is compared with the other implemented segmentation models on both datasets [30-45].

5.2. Proposed Segmentation Model

The proposed architecture is based on the ResNet50 model. ResNet50 is a residual-based deep learning model that uses skip connections. It utilizes four blocks, namely, input, convolutional, identity, and output blocks, as depicted in Figure 5(a). The convolutional and identity blocks are briefly described in Figure 5 (b) and (c), respectively [46-49].

To enhance its performance, an additional layer, that is, a dropout layer, is incorporated in the input stage. The dropout factor is set to 50%, and the ReLU activation function is replaced by the clipped ReLU to avoid overfitting. The Cliped-ResNet50 model exhibited the best performance among all models. The basic architecture of ResNet50 and the proposed Clipped-ResNet50 models is shown in Figure 6 (a) and (b), respectively.

In a clipped ReLU layer, a thresholding operation is performed where inputs less than zero are set to zero, and values greater than the clipping ceiling are set to the clipping ceiling. The mathematical model is given in equation 4 [50].

$$g(z) = \begin{cases} 0\,; & for\ z < 0 \\ z\,; & for\ 0 \le z < ceiling \\ ceiling\,; & for\ z \ge ceiling \end{cases} \quad (4)$$

The ceiling value is set to 10.

5.3. Performance Analysis of Various DL based Segmentation Methods

The performance of segmentation methods is evaluated in terms of accuracy and mIoU. The mean IOU and accuracy are calculated using equations 5 and 6 [51-53].

$$IOU = \frac{TP}{TP+FP+FN} \quad (5)$$

$$Accuracy = \frac{TP+TN}{TP+FP+TN+FN} \quad (6)$$

Where TP, TN, FP, and FN denote true positive, true negative, false positive, and false negative, respectively.

Table 5. Performance assessment of various DL based segmentation methods

Model	Dataset A (BUSI)		Dataset B (PGI Rohtak)	
	mIoU	Accuracy	mIoU	Accuracy
VGG19	0.8632	0.9212	0.7602	0.8834
Xception	0.8891	0.9230	0.8622	0.9132
ResNet18	0.8897	0.9245	0.8900	0.9245
MobilenetV2	0.8925	0.9249	0.8842	0.9262
ResNet50	0.8938	0.9270	0.8963	0.9280
Proposed Model Clipped-ResNet50	0.9089	0.9379	0.9060	0.9387

5.4. Statistical Analysis of Variance (ANOVA)

To determine a significant difference in the mIOU values between the experiments conducted on the BUSI and PGI Rohtak datasets, a one-way ANOVA test is performed. The mIOU values are grouped into two categories corresponding to the two experiments, and the null hypothesis for group mean values is tested. The resulting p-value for the mIOU is 0.3387. As the p-value exceeds 0.05, no statistically significant difference exists between the two experiments. The ANOVA diagram, along with the between-group and within-group variances, is presented in Figure 7 [54].

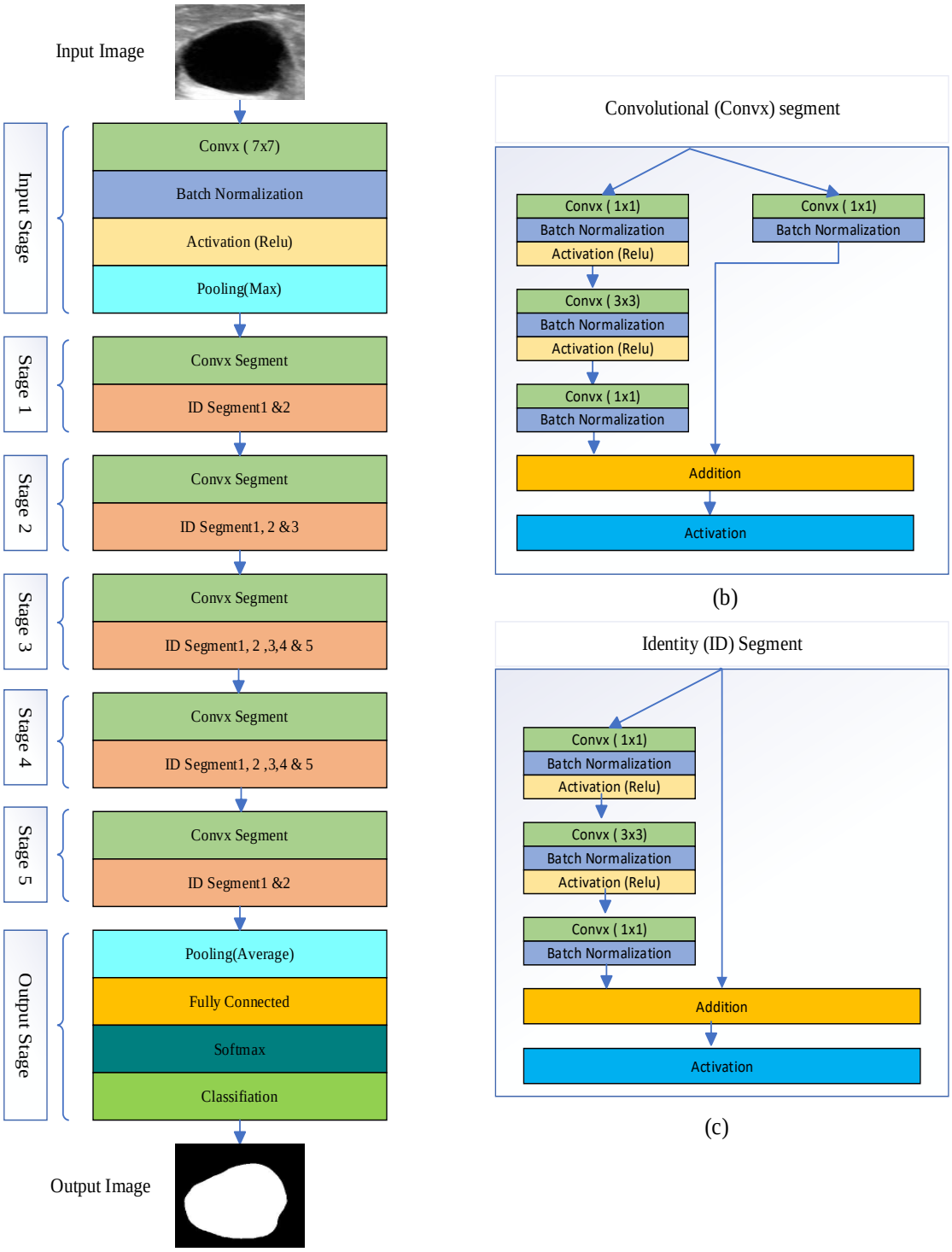

Fig. 5(a) Basic Resnet-50 model, (b) Convolutional segment, and (c) Identity segment.

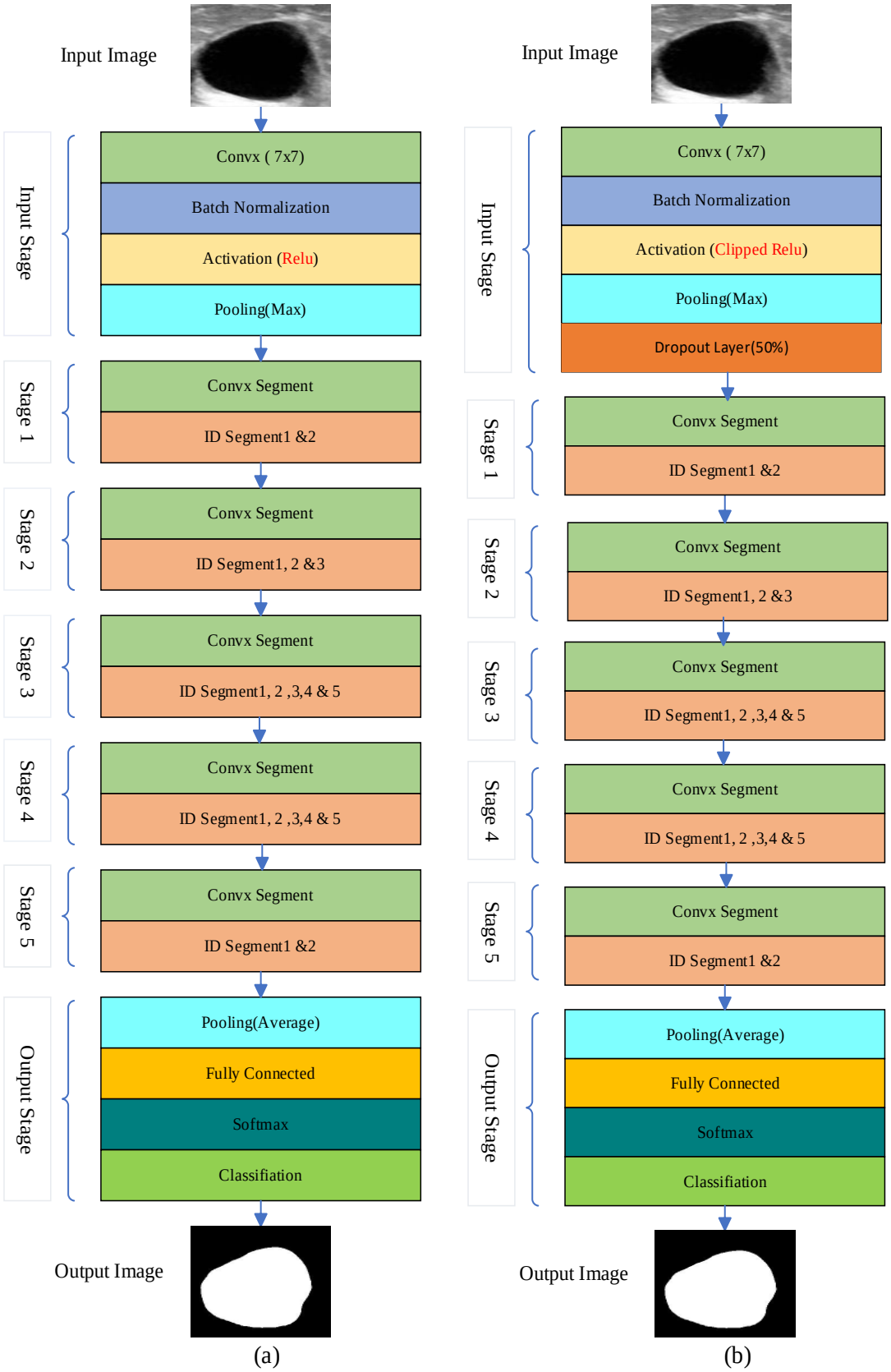

Fig. 6(a) ResNet50 basic architecture, and (b)Proposed ResNet50 based architecture: Clipped ResNet50

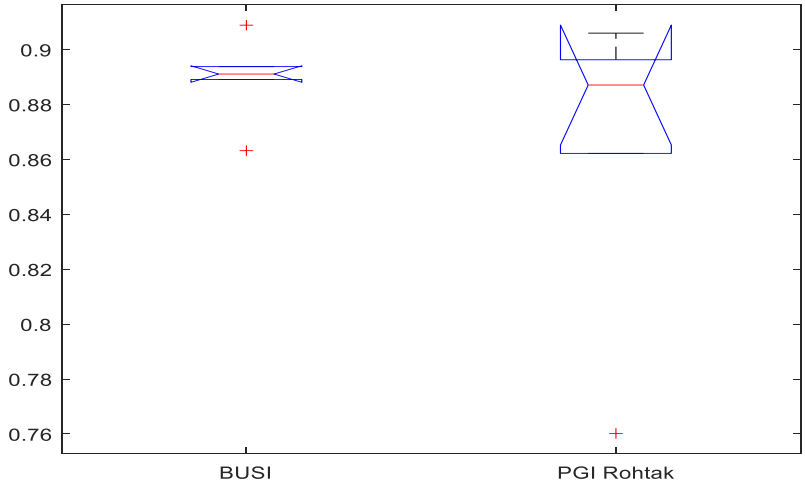

Fig.7 One-way ANOVA test on BUSI and PGI Rohtak datasets

6. Effect of Proposed Despeckling Algorithm (AD-BiF) on Proposed Segmentation Algorithm (Clipped-ResNet50) for BUS Images

In this study, segmentation is performed using the original and despeckled BUS images. The accuracy, Dice Similarity Coefficient (DSC), and mean IOU increased when despeckled images were used for segmentation, as shown in Table 6.

The results of the impact of noise on the proposed segmentation model are shown in Figure 8.

Table 6. Performance assessment of Clipped-ResNet50 on original and despeckled BUS images

Model	Dataset A			Dataset B		
	mIoU	DSC	Accuracy	mIoU	DSC	Accuracy
Original Images	0.9089	0.9437	0.9379	0.9060	0.9329	0.9387
Despeckled Images	0.9305	0.9573	0.9493	0.9289	0.9511	0.9536

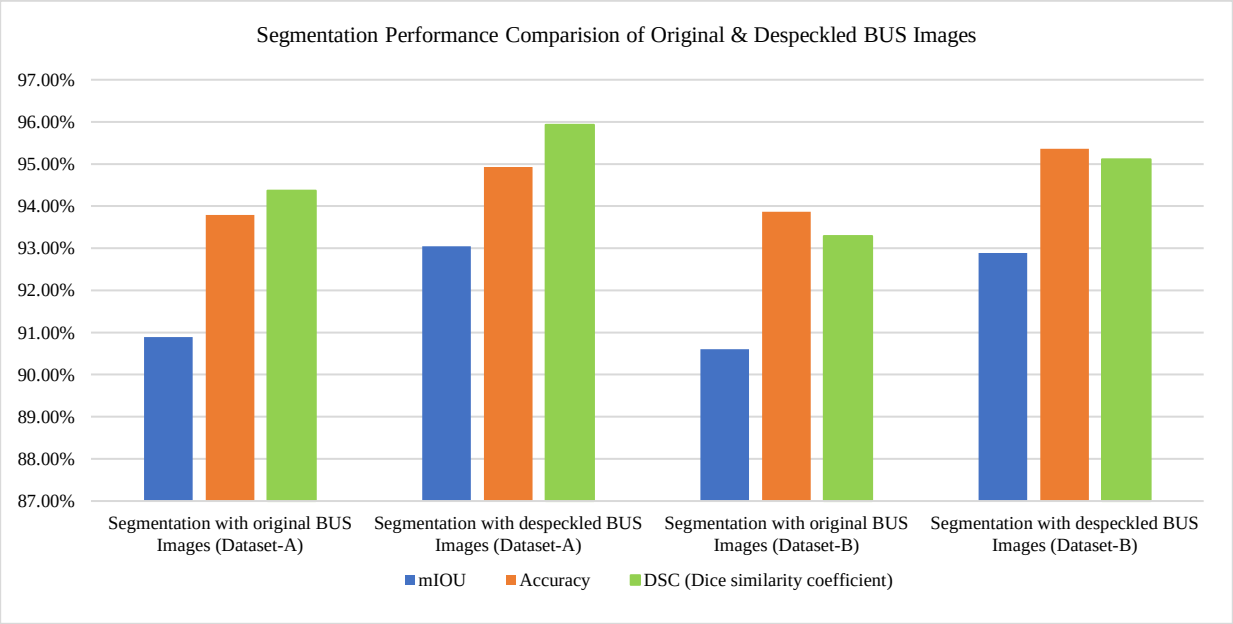

Fig. 8 The result of the impact of noise on the proposed segmentation model

7. Results and Discussion

In this study, various experiments are performed to achieve the best output of segmentation for BUS images. The detailed outcomes are as follows:

As described in section 2.2, for the preprocessing of BUS images, 15 different despeckling filters of various categories are applied to 2 different datasets of BUS images, and their performance is computed using the SEPI metric as presented in Table 2. It is observed that BiF, GeM, and AD filters achieved the best SEPI metric values from the basic, smoothing, and edge preserving filters categories.

Further, as described in section 2, six hybrid filters are constructed by fusing the information obtained from BiF, GeM, and AD filters. The performance of all these filters is shown in Table 3. From Table 3, it is observed that the AD-BiF filter achieved the 0.9818 ± 0.0241 and 0.9516 ± 0.1859 highest value of SEPI for dataset A and dataset B of BUS images.

For segmentation of BUS images, as described in section 4, Clipped-ResNet50 based DL model is proposed, and its performance is compared with VGG-19, Xception, ResNet18, MobileNetV2, and ResNet50 DL based models in terms of mean IOU and accuracy for both datasets of BUS images. From Table 5, it is observed that the proposed model (Clipped-ResNet50) achieved the highest mIOU and accuracy values in comparison to other techniques. In addition to this, to determine the statistical correlation between the two datasets, one one-way ANOVA test is also performed.

Performance of the proposed segmentation model is also compared with existing research findings, as shown in Table 7. It is noticed that the proposed model achieved the highest value of mIOU and accuracy.

Both the original and filtered Breast Ultrasound (BUS) images are carefully reviewed along with lesion annotations performed under the guidance of an experienced radiologist. The overlap between the segmented regions in the original and despeckled BUS images is evaluated using ground-truth images by calculating the mean IOU.

The analysis demonstrates that the despeckled images result in improved segmentation performance compared with the original BUS images. The original BUS images with masks and the segmented images with masks from datasets A and B are depicted in Figure 9.

Table 7. Performance comparison of the proposed segmentation model with existing research

Author	Dataset	Segmentation Model	Performance parameters
Bruno et al. [32]	BUSI	Dual stage DL based	Acc.=91.50%
Hesaraki et al. [37]	BUSI	UNet+++ LSTM hybrid	mIOU=0.84
Proposed	BUSI	Clipped-Resnet50	Acc.=93.79% mIOU=0.9089

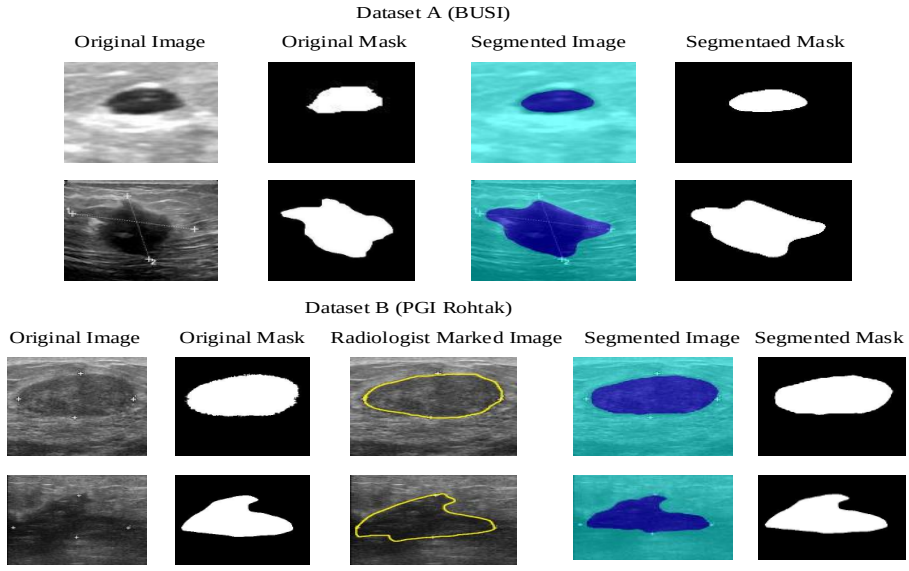

Fig. 9 Breast ultrasound images with mask & corresponding segmented image with segmented mask

8. Conclusion

In this research, a BUS image segmentation approach was proposed, comprising two primary modules: a despeckling stage and a segmentation stage. For the despeckling task, a Hybrid Adaptive Filter (AD-BiF) was introduced and evaluated in comparison to existing filters. The experimental results demonstrated that AD-BiF achieved the highest SEPI values of 0.9818 and 0.9516 for Datasets A and B, respectively, indicating superior speckle noise reduction. Subsequently, an enhanced segmentation network, termed Clipped-ResNet50, was developed by modifying the ResNet50 architecture. The segmentation results revealed that the proposed model, i.e., Clipped-ResNet50, yielded a higher performance, achieving mean IOU values of 0.9089 for Dataset A and 0.9060 for Dataset B. Furthermore, a comparative analysis between the segmentation of the original and despeckled images was conducted. The findings highlighted that the despeckled images significantly improved segmentation accuracy. Specifically, for the BUSI dataset, the mean IOU, accuracy, and DSC increased from 90.89% to 93.05%, 93.79% to 94.93%, and 94.37% to 95.73%, respectively. Similarly, for the PGI dataset, the mean IOU, accuracy, and DSC increased from 90.60% to 92.89%, 93.87% to 95.36%, and 93.29% to 95.11%, respectively. Overall, the proposed framework demonstrates that combining effective despeckling with a robust DL–based segmentation model can substantially enhance the accuracy of BUS image segmentation.

References

[1] Kathryn P. Trayes, and Sarah E.H. Cokenakes, "Breast Cancer Treatment," *American Family Physician*, vol. 104, no. 2, pp. 171-178, 2021. [Google Scholar] [Publisher Link]

[2] Melina Arnold et al., "Current and Future Burden of Breast Cancer: Global Statistics for 2020 and 2040," *The Breast*, vol. 66, pp. 15-23, 2022. [CrossRef] [Google Scholar] [Publisher Link]

[3] Mohammad Madani, Mohammad Mahdi Behzadi, and Sheida Nabavi, "The Role of Deep Learning in Advancing Breast Cancer Detection using Different Imaging Modalities: A Systematic Review," *Cancers*, vol. 14, no. 21, pp. 1-36, 2022. [CrossRef] [Google Scholar] [Publisher Link]

[4] Athar Shams Rana, Javairia Rafique, and Hira Riffat, *Advances in Breast Ultrasound Imaging: Enhancing Diagnostic Precision and Clinical Utility*, Latest Research on Breast Cancer, 2024. [CrossRef] [Google Scholar] [Publisher Link]

[5] Wilfrido Gómez Flores et al., "Breast Ultrasound Despeckling using Anisotropic Diffusion Guided by Texture Descriptors," *Ultrasound in Medicine & Biology*, vol. 40, no. 11, pp. 2609-2621, 2014. [CrossRef] [Google Scholar] [Publisher Link]

[6] Iman Elyasi et al., "Speckle Reduction in Breast Cancer Ultrasound Images by using Homogeneity Modified Bayes Shrink," *Measurement*, vol. 91, pp. 55-65, 2016. [CrossRef] [Google Scholar] [Publisher Link]

[7] Kriti, Jitendra Virmani, and Ravinder Agarwal, "Assessment of Despeckle Filtering Algorithms for Segmentation of Breast Tumours from Ultrasound Images," *Biocybernetics and Biomedical Engineering*, vol. 39, no. 1, pp. 100-121, 2019. [CrossRef] [Google Scholar] [Publisher Link]

[8] Hyunho, and Jechang Jeong, "Despeckling Algorithm for Removing Speckle Noise from Ultrasound Images," *Symmetry*, vol. 12, no. 6, pp. 1-26, 2020. [CrossRef] [Google Scholar] [Publisher Link]

[9] Gelan Ayana et al., "De-Speckling Breast Cancer Ultrasound Images using a Rotationally Invariant Block Matching Based Non-Local Means (RIBM-NLM) Method," *Diagnostics*, vol. 12, no. 4, pp. 1-17, 2022. [CrossRef] [Google Scholar] [Publisher Link]

[10] Niranjan Yadav, Rajeshwar Dass, and Jitendra Virmani, "Despeckling Filters Applied to Thyroid Ultrasound Images: A Comparative Analysis," *Multimedia Tools and Applications*, vol. 81, pp. 8905-8937, 2022. [CrossRef] [Google Scholar] [Publisher Link]

[11] Tong Ying et al., "Breast Ultrasound Image Despeckling using Multi-Filtering DFrFT and Adaptive Fast BM3D," *Computer Methods and Programs in Biomedicine*, vol. 246, 2024. [CrossRef] [Google Scholar] [Publisher Link]

[12] Dongkyu Jung et al., "Unsupervised Speckle Noise Reduction Technique for Clinical Ultrasound Imaging," *Ultrasonography*, vol. 43, no. 5, pp. 327-344, 2024. [CrossRef] [Google Scholar] [Publisher Link]

[13] Xiangyu Li et al., "A Detail-Preserving Ultrasound Speckle Reduction Method Based on Complementary Information," *Ultrasound in Medicine & Biology*, vol. 52, no. 1, pp. 108-122, 2026. [CrossRef] [Google Scholar] [Publisher Link]

[14] Mostafa Khalifa, Hanaa M. Hamza, and Khalid M. Hosny, "De-speckling of Medical Ultrasound Image using Metric-Optimized Knowledge Distillation," *Scientific Reports*, vol. 15, pp. 1-21, 2025. [CrossRef] [Google Scholar] [Publisher Link]

[15] M.S. Gokmen et al., "An Effective Image Despeckling and Reconstruction Approach using U-Net based Model and Comparative Analysis," *Scientific Reports*, vol. 15, pp. 1-21, 2025. [CrossRef] [Google Scholar] [Publisher Link]

[16] Nilima Patil, M.M. Deshpande, and V.N. Pawar, "A Novel Deep Learning Approach for Speckle Denoising Using Hyperparameter Tuning," *Journal of Image and Graphics*, vol. 13, no. 3, pp. 267-274, 2025. [CrossRef] [Google Scholar] [Publisher Link]

[17] Vijaya S. Patil et al., "Despeckeling Method for Ultrasound Thyroid Nodules Using Innovative Wiener Filter," *Proceedings of the 3rd International Conference on Futuristic Technology*, vol. 2, pp. 885-889, 2025. [CrossRef] [Google Scholar] [Publisher Link]

[18] Walid Al-Dhabyani, *Dataset of Breast Ultrasound Images*, Data in Brief, vol. 28, pp. 1-5, 2020. [CrossRef] [Google Scholar] [Publisher Link]

[19] Fatima M. Osman, and Moi Hoon Yap, "The Effect of Filtering Algorithms for Breast Ultrasound Lesions Segmentation," *Informatics in Medicine Unlocked*, vol. 12, pp. 14-20, 2018. [CrossRef] [Google Scholar] [Publisher Link]

[20] Ju Zhang, Chen Wang, and Yun Cheng, "Comparison of Despeckle Filters for Breast Ultrasound Images," *Circuits, Systems, and Signal Processing*, vol. 34, pp. 185-208, 2015. [CrossRef] [Google Scholar] [Publisher Link]

[21] Jong-Sen Lee, "Speckle Analysis and Smoothing of Synthetic Aperture Radar Images," *Computer Graphics and Image Processing*, vol. 17, no. 1, pp. 24-32, 1981. [CrossRef] [Google Scholar] [Publisher Link]

[22] Darwin T. Kuan et al., "Adaptive Noise Smoothing Filter for Images with Signal-Dependent Noise," *IEEE Transactions on Pattern Analysis and Machine Intelligence*, vol. 7, no. 2, pp. 165-177, 1985. [CrossRef] [Google Scholar] [Publisher Link]

[23] Victor S. Frost et al., "A Model for Radar Images and its Application to Adaptive Digital Filtering of Multiplicative Noise," *IEEE Transactions on Pattern Analysis and Machine Intelligence*, vol. 4, no. 2, pp. 157-166, 1982. [CrossRef] [Google Scholar] [Publisher Link]

[24] P. Perona, and J. Malik, "Scale-Space and Edge Detection Using Anisotropic Diffusion," *IEEE Transactions on Pattern Analysis and Machine Intelligence*, vol. 12, no. 7, pp. 629-639, 1990. [CrossRef] [Google Scholar] [Publisher Link]

[25] Irraivan Elamvazuthi, Muhammad Luqman Bin Muhd Zain, and K.M. Begam, "Despeckling of Ultrasound Images of Bone Fracture using Multiple Filtering Algorithms," *Mathematical and Computer Modelling*, vol. 57, no. 1-2, pp. 152-168, 2013. [CrossRef] [Google Scholar] [Publisher Link]

[26] Joachim Weickert, "Coherence-Enhancing Diffusion Filtering," *International Journal of Computer Vision*, vol. 31, pp. 111-127, 1999. [CrossRef] [Google Scholar] [Publisher Link]

[27] Sean Finn, Martin Glavin, and Edward Jones, "Echocardiographic Speckle Reduction Comparison," *IEEE Transactions on Ultrasonics, Ferroelectrics, and Frequency Control*, vol. 58, no. 1, pp. 82-101, 2011. [CrossRef] [Google Scholar] [Publisher Link]

[28] Rajeshwar Dass, and Niranjan Yadav, "Image Quality Assessment Parameters for Despeckling Filters," *Procedia Computer Science*, vol. 167, pp. 2382-2392, 2020. [CrossRef] [Google Scholar] [Publisher Link]

[29] S. Senthil Kumar, and S. Muttan, "PCA-based Image Fusion," *Algorithms and Technologies for Multispectral, Hyperspectral, and Ultraspectral Imagery XII*, vol. 6233, 2006. [CrossRef] [Google Scholar] [Publisher Link]

[30] Samuel E. Johnny et al., "Prompt-Free SAM-Based Multi-Task Framework for Breast Ultrasound Lesion Segmentation and Classification," *arXiv preprint*, pp. 1-6, 2026. [CrossRef] [Google Scholar] [Publisher Link]

[31] Yajuan Li et al., "Deep Learning Based on Ultrasound Images Differentiates Parotid Gland Pleomorphic Adenomas and Warthin Tumors," *Ultrasonic Imaging*, vol. 47, no. 3-4, 2025. [CrossRef] [Google Scholar] [Publisher Link]

[32] Pierangela Bruno, Megan Macrì, and Carmine Dodaro, "A Dual-Stage Deep Learning Framework for Breast Ultrasound Image Segmentation and Classification," *Journal of Medical Systems*, vol. 49, pp. 1-11, 2025. [CrossRef] [Google Scholar] [Publisher Link]

[33] Mohammad Amanour Rahman, "HyFormer-Net: A Synergistic CNN-Transformer with Interpretable Multi-Scale Fusion for Breast Lesion Segmentation and Classification in Ultrasound Images," *arXiv preprint*, pp. 1-16, 2025. [CrossRef] [Google Scholar] [Publisher Link]

[34] Lal Omega Boro, and Gypsy Nandi, "CBAM-RIUnet: Breast Tumor Segmentation with Enhanced Breast Ultrasound and Test-Time Augmentation," *Ultrasonic Imaging*, vol. 47, no. 1, pp. 24-36, 2024. [CrossRef] [Google Scholar] [Publisher Link]

[35] Golla Madhu et al., "UCapsNet: A Two-Stage Deep Learning Model Using U-Net and Capsule Network for Breast Cancer Segmentation and Classification in Ultrasound Imaging," *Cancers*, vol. 16, no. 22, pp. 1-20, 2024. [CrossRef] [Google Scholar] [Publisher Link]

[36] Payel Pramanik et al., "DAU-Net: Dual Attention-aided U-Net for Segmenting Tumor in Breast Ultrasound Images," *Plos one*, vol. 19, no. 5, pp. 1-20, 2024. [CrossRef] [Google Scholar] [Publisher Link]

[37] Saba Hesaraki, Morteza Akbari, and Ramin Mousa, "UNet++ and Lstm Combined Approach for Breast Ultrasound Image Segmentation," *arXiv preprint*, pp. 1-16, 2024. [CrossRef] [Google Scholar] [Publisher Link]

[38] Yuchao Lyu et al., "AMS-PAN: Breast Ultrasound Image Segmentation Model Combining Attention Mechanism and Multi-Scale Features," *Biomedical Signal Processing and Control*, vol. 81, pp. 1-13, 2023. [CrossRef] [Google Scholar] [Publisher Link]

[39] Haonan Yang, and Dapeng Yang, "CSwin-PNet : A CNN-Swin Transformer Combined Pyramid Network for Breast Lesion Segmentation in Ultrasound Images," *Expert Systems with Applications*, vol. 213, 2023. [CrossRef] [Google Scholar] [Publisher Link]

[40] Tianyu Zhao, and Hang Dai, "Breast Tumor Ultrasound Image Segmentation Method Based on Improved Residual U-Net Network," *Computational Intelligence and Neuroscience*, vol. 2022, no. 1, pp. 1-9, 2022. [CrossRef] [Google Scholar] [Publisher Link]

[41] Jaeil Kim et al., "Weakly - Supervised Deep Learning for Ultrasound Diagnosis of Breast Cancer," *Scientific Reports*, vol. 11, pp. 1-10, 2021. [CrossRef] [Google Scholar] [Publisher Link]

[42] Kuan Huang et al., "Shape-Adaptive Convolutional Operator for Breast Ultrasound Image Segmentation," *2021 IEEE International Conference on Multimedia and Expo (ICME)*, Shenzhen, China, pp. 1-6, 2021. [CrossRef] [Google Scholar] [Publisher Link]

[43] Ademola Enitan Ilesanmi, Utairat Chaumrattanakul, and Stanislav S. Makhanov, "A Method for Segmentation of Tumors in Breast Ultrasound Images using the Variant Enhanced Deep Learning," *Biocybernetics and Biomedical Engineering*, vol. 41, no. 2, pp. 802-818, 2021. [CrossRef] [Google Scholar] [Publisher Link]

[44] Wilfrido Gómez-Flores, and Wagner Coelho de Albuquerque Pereira, "A Comparative Study of Pre-trained Convolutional Neural Networks for Semantic Segmentation of Breast Tumors in Ultrasound," *Computers in Biology and Medicine*, vol. 126, 2020. [CrossRef] [Google Scholar] [Publisher Link]

[45] Sarita, and Rajeshwar Dass, "A Hybrid Model for Brain Tumor Classification via Deep Feature Extraction and Optimized Classifier Weighting," *Biomedical Physics & Engineering Express*, vol. 11, no. 5, 2025. [CrossRef] [Google Scholar] [Publisher Link]

[46] Hailong Yang, Yinghao Liu, and Tian Xia, "Defect Detection Scheme of Pins for Aviation Connectors based on Image Segmentation and Improved RESNET-50," *International Journal of Image and Graphics*, vol. 24, no. 1, 2024. [CrossRef] [Google Scholar] [Publisher Link]

[47] Shoffan Saifullah et al., "Automatic Brain Tumor Segmentation: Advancing U-Net with ResNet50 Encoder for Precise Medical Image Analysis," *IEEE Access*, vol. 13, pp. 43473-43489, 2025. [CrossRef] [Google Scholar] [Publisher Link]

[48] Qinghua Huang et al., "Segmentation of Breast Ultrasound Image with Semantic Classification of Superpixels," *Medical Image Analysis*, vol. 61, 2020. [CrossRef] [Google Scholar] [Publisher Link]

[49] Ji Yang, Mehdi Faraji, and Anup Basu, "Robust Segmentation of Arterial Walls in Intravascular Ultrasound Images using Dual Path U-Net," *Ultrasonics*, vol. 96, pp. 24-33, 2019. [CrossRef] [Google Scholar] [Publisher Link]

[50] Animesh Karnewar et al., "ReLU Fields: The Little Non-Linearity that Could," *ACM SIGGRAPH 2022 Conference Proceedings*, pp. 1-9, 2022. [CrossRef] [Google Scholar] [Publisher Link]

[51] Jignesh Chowdary et al., "A Multi-Task Learning Framework for Automated Segmentation and Classification of Breast Tumors from Ultrasound Images," *Ultrasonic Imaging*, vol. 44, no. 1, pp. 3-12, 2022. [CrossRef] [Google Scholar] [Publisher Link]

[52] Niranjan Yadav, Rajeshwar Dass, and Jitendra Virmani, "Machine Learning-Based CAD System for Thyroid Tumour Characterisation using Ultrasound Images," *International Journal of Medical Engineering and Informatics*, vol. 16, no. 6, pp. 547-559, 2024. [CrossRef] [Google Scholar] [Publisher Link]

[53] Niranjan Yadav, Rajeshwar Dass, and Jitendra Virmani, "Assessment of Encoder-Decoder-Based Segmentation Models for Thyroid Ultrasound Images," *Medical & Biological Engineering & Computing*, vol. 61, pp. 2159-2195, 2023. [CrossRef] [Google Scholar] [Publisher Link]

[54] Sanggyu Kwak, "Are Only p-Values Less than 0.05 Significant? A p-Value Greater Than 0.05 Is Also Significant!," *Journal of Lipid and Atherosclerosis*, vol. 12, no. 2, pp. 89-95, 2023. [CrossRef] [Google Scholar] [Publisher Link]